5436 *Biochemistry* **2010,** *49,* 5436–5444
DOI: 10.1021/bi100558z

BIOCHEMISTRY
including biophysical chemistry & molecular biology
Article

Biophysical Characterization of Iron in Mitochondria Isolated from Respiring and Fermenting Yeast[†]

Jessica Garber Morales,[‡] Gregory P. Holmes-Hampton,[‡] Ren Miao,[‡] Yisong Guo,[§] Eckard Münck,[§] and Paul A. Lindahl*[,‡,∥]

[‡]*Department of Chemistry, Texas A&M University, College Station, Texas 77843-3255,* [§]*Department of Chemistry, Carnegie Mellon University, Pittsburgh, Pennsylvania 15213, and* [∥]*Department of Biochemistry and Biophysics, Texas A&M University, College Station, Texas 77843*

Received April 12, 2010; Revised Manuscript Received May 30, 2010

ABSTRACT: The distributions of Fe in mitochondria isolated from respiring, respiro-fermenting, and fermenting yeast cells were determined with an integrative biophysical approach involving Mössbauer and electronic absorption spectroscopies, electron paramagnetic resonance, and inductively coupled plasma emission mass spectrometry. Approximately 40% of the Fe in mitochondria from respiring cells was present in respiration-related proteins. The concentration and distribution of Fe in respiro-fermenting mitochondria, where both respiration and fermentation occur concurrently, were similar to those of respiring mitochondria. The concentration of Fe in fermenting mitochondria was also similar, but the distribution differed dramatically. Here, levels of respiration-related Fe-containing proteins were diminished ~3-fold, while non-heme HS Fe^{II} species, non-heme mononuclear HS Fe^{III}, and Fe^{III} nanoparticles dominated. These changes were rationalized by a model in which the pool of non-heme HS Fe^{II} ions serves as feedstock for Fe−S cluster and heme biosynthesis. The integrative approach enabled us to estimate the concentration of respiration-related proteins.

Mitochondria are cellular organelles that play critical roles in cellular physiology. Respiration and oxidative phosphorylation occur in these organelles, as do heme biosynthesis and iron−sulfur cluster assembly. As such, mitochondria are "hubs" of cellular iron trafficking (*3*). The Fe^{II} ions used for these processes are imported by Mrs3p and Mrs4p, high-affinity transporters on the IM[1] (*3*). Once in the matrix, these ions are delivered to Fe−S scaffold proteins and ferrochelatase (*3*). Many of these Fe−S and heme centers are inserted into respiratory complexes. Succinate dehydrogenase contains one $[Fe_2S_2]$, $[Fe_3S_4]$, and $[Fe_4S_4]$ cluster each as well as a LS heme *b* (*4*). Cytochrome bc_1 contains two LS *b* type hemes, one LS *c* heme, and a Rieske $[Fe_2S_2]$ cluster (*5*). Cytochrome *c* contains one LS heme *c*. Cytochrome *c* oxidase contains two heme *a* molecules and three Cu ions (*6*). Other mitochondrial proteins contain $[Fe_4S_4]$ and $[Fe_2S_2]$ clusters, hemes, and non-heme Fe^{II} ions (see ref *1* for a list of mitochondrial Fe-containing proteins).

Mitochondrial dysfunction is associated with aging and various diseases, including cancer, heart disease, anemia, and neurodegeneration (*7*−*9*). As cells age, there is a decline in the level of Fe−S cluster biogenesis and mitochondrial membrane potential, leading with higher probability to a cellular crisis associated with loss of mitochondrial DNA, the instability and hypermutability of nuclear DNA, and cancer (*10*). Aged cells exhibit signs of iron starvation (*10*). Reactive oxygen species (ROS) generated by Fe centers within the mitochondria may damage the DNA and other cellular components (*11*), causing apoptosis (*12*−*14*). Ferrous ions are particularly adept at producing ROS via Fenton chemistry (*15*). In Friedreich's ataxia, the level of mitochondrial frataxin is depleted, causing a buildup of iron in the organelle (*16*−*19*). In Parkinson's disease, there is a buildup of Fe in the *substantia nigra* portion of the brain (*20*, *21*). Patients with sideroblastic anemia accumulate Fe that cannot be incorporated into hemoglobin (*3*, *22*).

Much progress in understanding cellular function has been made by "omics"-level studies in which entire subsets of cellular components are measured simultaneously and analyzed as a system (*23*). We have developed an integrative biophysical approach centered on Mössbauer spectroscopy to study the systems-level distribution of iron within cells and organelles (*2*). ^{57}Fe Mössbauer spectroscopy detects all Fe species in a sample, with spectral intensities proportional to relative Fe concentrations (*24*). In complex systems, Mössbauer generally cannot resolve individual Fe species, but it can identify groups of such species. This is not ideal, but the resolution of Fe species can be enhanced by EPR, which can detect paramagnetic species, electronic absorption spectroscopy, which can quantify heme chromophores, and ICP-MS, which can quantify the overall Fe concentration.

In this study, we have assessed the Fe content of mitochondria isolated from yeast grown under fermenting, respiro-fermenting, and respiring conditions. Mitochondria play a dominant role in respiration but not fermentation; however, they are essential for cell viability regardless of metabolic growth mode. Fermenting cells produce fewer mitochondria than respiring cells. Early in the exponential growth phase, fermenting cells are largely devoid of mitochondria; in later stages, the organelle occupies ~3% of the

[†]This study was supported by National Institutes of Health Grants GM084266, (P.A.L.), EB-001475 (E.M.), and T32GM008523 (G.P.H.-H. and J.G.-M.) and the Robert A. Welch Foundation (Grant A1170 to P.A.L.).

*To whom correspondence should be addressed. Phone: (979) 845-0956. Fax: (979) 845-4719. E-mail: lindahl@chem.tamu.edu.

[1]Abbreviations: HS, high-spin; LS, low-spin; NHHS, non-heme high-spin; IM, inner membrane; EPR, electron paramagnetic resonance; ICP-MS, inductively coupled plasma emission mass spectrometry.

 Published on Web 06/10/2010

cell volume (*25*). Under respiration, mitochondria represent ~10% of the cell volume. Mitochondria in yeast are present as a large tubular network (*26*); the network from fermenting cells is thinner and less branched.

We report here that respiration-related Fe-containing proteins and other $[Fe_4S_4]^{2+}$ cluster-containing proteins dominate the iron content of mitochondria from respiring and respiro-fermenting cells. Under fermention, the concentrations of these species decline while those of non-heme high-spin (NHHS) Fe^{II} ions, mononuclear HS Fe^{III} ions, and Fe^{III} nanoparticles increase. These changes can be rationalized by assuming that the NHHS Fe^{II} ions constitute a pool used for Fe−S cluster and heme biosynthesis.

EXPERIMENTAL PROCEDURES

Cultures (25 L) of W303-1B cells were grown on minimal medium (*27*) with 3% (v/v) glycerol (batches R1, R2, R4, and R5), 2% (w/v) galactose (batches RF1 and RF2), or 2% (w/v) glucose (batches F5−F16). See Table S1 of the Supporting Information for a listing of all batches used in this study. Respiring batches were supplemented with 10% YPG medium except for R3 which was grown on YPG. Batches F1−F4 were grown on YPD (*28*) instead of minimal medium. Batches were supplemented with 40 μM ^{57}Fe as described previously (*27*), except RF1 which was supplemented with 20 μM ^{57}Fe. Mitochondria were isolated, packed, and frozen in the as-isolated state, as described previously (*1*, *2*), without the addition of reductants or oxidants. In our current samples, dithionite is less able to reduce spectral components, relative to the effect reported previously (*1*). See ref *29* for current Mössbauer spectra of dithionite-treated mitochondria. In earlier batches, dithionite reduced the Fe in approximately half of the central doublet, whereas in our current samples, dithionite had little effect [as the central quadrupole doublet comprises low-spin Fe(II) hemes and $[Fe_4S_4]^{2+}$ clusters, dithionite would act on the latter]. We are uncertain why our samples have become insensitive to dithionite, but we suspect that the negatively charged dithionite ion cannot cross the IM, suggesting that only mitochondria with broken membranes can be reduced. In our current samples, a higher proportion of membranes may be intact. Intactness was evaluated by protease protection assays as described previously (*30*).

Protein and metal concentrations were determined as described previously (*1*) except that 1−2% deoxycholate was used to disrupt membranes, and the bicinchoninic acid method (Thermo Scientific) was used to determine protein concentrations. The protein concentrations of packed mitochondria reported in this study were higher by a factor of ~2 relative to our previous determinations (*1*). Current samples were treated with deoxycholate rather than being sonicated prior to protein concentration determinations, and this may have released additional proteins from membranes and/or reduced the extent of protein degradation. The current metal:protein ratios (~4 nmol of Fe/mg of protein) for respiring and respiro-fermenting mitochondria are similar to those reported from other laboratories (*16*, *31*−*34*), and thus, we consider our current protein concentrations to be more accurate.

EPR and Mössbauer measurements were performed as described previously (*1*, *27*). Low temperature spectra collected at Texas A&M University varied from 4.5 K to 6 K, but these differences, relative to the 4.2 K spectra collected at Carnegie Mellon University, do not alter simulations significantly. For electronic absorption spectroscopy, samples were resuspended in 0.6 M sorbitol and 20 mM HEPES (pH 7.4); spectra were obtained as described previously (*2*). Spectra of human cytochrome b_5 [Sigma, 18 μM in a buffer composed of 1.2 M sorbitol, 50 mM Tris (pH 8.5) and 1 mM dithionite] and yeast cytochrome *c* (Sigma, 20 μM in the same buffer) were also collected. The digital spectrum of bovine heart cytochrome *c* oxidase (*35*) was provided by G. Palmer (Rice University, Houston, TX). Absorbances were normalized to a 1 cm path length and divided by molar protein concentrations. Extinction coefficients for cytochrome *c* oxidase were divided by 2 to account for there being two heme *a* groups per protein. The resulting wavelength-dependent extinction coefficients [$\varepsilon_a(\lambda)$, $\varepsilon_b(\lambda)$, and $\varepsilon_c(\lambda)$] for hemes *a*, *b*, and *c*, respectively, are shown in Figure S1 of the Supporting Information. Spectra were analyzed using OriginPro (www.originlab.com) and the relationship

$$\mathrm{Abs}(\lambda) = [\text{heme } a]\varepsilon_a(\lambda) + [\text{heme } b]\varepsilon_b(\lambda) + [\text{heme } c]\varepsilon_c(\lambda) + \text{light scattering}$$

Table 1: Analytical Properties of Isolated Mitochondria[a]

	respiring	respiro-fermenting	fermenting
[protein] (mg/mL)	170 ± 61 (5)	200 ± 60 (2)	110 ± 30 (11)
[Fe] (μM)	720 ± 210 (5)	840 ± 120 (2)	770 ± 320 (11)
[Cu] (μM)	210 ± 170 (5)	160 ± 80 (2)	50 ± 37 (11)
[Mn] (μM)	35 ± 20 (5)	12 ± 4 (2)	15 ± 12 (11)
[Zn] (μM)	290 ± 160 (5)	230 ± 150 (2)	290 ± 210 (11)
central doublet	60 ± 2% (2)	50% (1)	25 ± 4% (5)
HS Fe^{II} heme	7 ± 1% (2)	4% (1)	4 ± 1% (5)
NHHS Fe^{II}	2 ± 1% (2)	3% (1)	20 ± 5% (5)
HS Fe^{III}	0 (2)	5% (1)	15 ± 3% (3)
$S = 1/2$ $[Fe_2S_2]^{+}$	13 ± 2% (2)	10% (1)	~0% (5)
$[Fe_2S_2]^{2+}$	< 5% (2)	< 5% (1)	~0% (5)
Fe^{III} nanoparticles	< 5% (2)	< 5% (1)	33 ± 7% (5)
unassigned Fe	~20%	~25%	~5% (5)
[Fe^{II} heme *a*] (μM)	51 ± 8 (4)	61 (1)	14 ± 1 (4)
[Fe^{II} heme *b*] (μM)	52 ± 8 (4)	55 (1)	27 ± 5 (4)
[Fe^{II} heme *c*] (μM)	120 ± 10 (4)	160 (1)	73 ± 15 (4)
$g_{ave} = 1.95$ (μM)	1−10 (3)	13 ± 4 (2)	1−3 (2)
$g_{ave} = 1.90$ (μM)	13 ± 3 (3)	29 ± 18 (2)	6 ± 2 (2)
$g = 2.01$ (μM)	0−1 (3)	1−2 (2)	0 (2)
$g = 2.00$ (μM)	0−2 (3)	0−6 (2)	0−1 (2)
$g = 2.04$ (μM)	1−3 (3)	3 ± 1 (2)	1−2 (2)
$g = 4.3$ (μM)	5−45 (3)	2−14 (2)	3 (1)
$g = 5.8$ (μM)	1−2 (3)	0−2 (2)	~0 (1)
$g = 6.4, 5.3$ (μM)	1−4 (3)	0−5 (2)	1 (1)
cytochrome *c* oxidase	30	35	8
succinate dehydrogenase	5	10	2
cytochrome bc_1	10	20	6
cytochrome *c*	100	140	60
other HS heme *b*	20	minor	minor
other LS hemes combined	180	230	100
other $[Fe_4S_4]^{2+}$ only	55	36	13
other $[Fe_4S_4]^{2+}$ + $[Fe_2S_2]^{+}$	minor	minor	minor
other $[Fe_2S_2]^{2+}$ only	minor	minor	minor
Cu^{I} pool	120	60	30

[a] In the top part, concentrations are for "neat" mitochondria (devoid of residual interstitial solvent). Experimentally determined protein and metal concentrations of mitochondrial suspensions were multiplied by the dilution factor used to prepare these samples from the packed state. Concentrations were also divided by 0.82, the packing efficiency (*1*, *2*). Values in the table are the average of the individual determinations given in Table S1 of the Supporting Information; the number of samples evaluated is in parentheses. Indicated relative uncertainties reflect variations between samples; additional uncertainties related to fitting are estimated to be ±20%. Heme *a*, *b*, and *c* concentrations were determined from electronic absorption spectra. Entries obtained by Mössbauer spectroscopy are given as a percentage of total Fe. Percentages of HS Fe^{III} species were determined only from 8.0 T Mössbauer spectra. The bottom part lists estimated concentrations of dominating Fe- and Cu-containing species in yeast mitochondria (in micromolar).

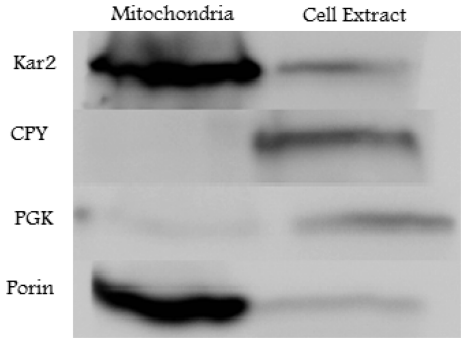

FIGURE 1: Western blot of EGTA-washed isolated mitochondria (left) and the corresponding extract (right) from respiring cells (batch R5). In both cases, 60 μg of protein was loaded into the wells of a 10% SDS−PAGE gel. Kar2 is an endoplasmic reticular protein (level increased 5-fold in isolated mitochondria vs cell extract). CPY is a vacuolar protein (level decreased 6-fold). PGK is a cytosolic protein (level decreased 5-fold). Porin is a mitochondrial protein (level increased 10-fold).

where [heme *a*], [heme *b*], and [heme *c*] are the concentrations of each heme center in the mitochondrial suspension. Concentrations were adjusted manually to obtain the composite spectra shown in Figure 3, using parameters listed in Table 1.

RESULTS

Respiring Mitochondria. Western blots of mitochondria isolated from respiring cells showed a 10-fold enrichment of the mitochondrial porin relative to that in cell extracts (Figure 1). Since ~10% of the volume of respiring yeast cells is occupied by mitochondria (*25*), this observation indicates that our samples were relatively pure. The membranes of isolated mitochondria were largely intact, in that the IMS protein cytochrome *c* was protected from proteinase K-catalyzed hydrolysis unless deoxycholate was added to disrupt membranes (Figure S2 of the Supporting Information). The metal content of samples was determined by ICP-MS (averages in Table 1 and individual determinations in Table S1 of the Supporting Information).

Low-field Mössbauer spectra of respiring mitochondria were dominated by the "central doublet" (Figure 2C, blue line). This doublet [60% of Fe (Table 1)] has an isomer shift δ of $\approx$0.45 mm/s and a quadrupole splitting ΔE_Q of $\approx$1.15 mm/s, parameters characteristic of both $S = 0$ $[Fe_4S_4]^{2+}$ clusters and LS Fe^{II} hemes. A minor contribution of $S = 0$ $[Fe_2S_2]^{2+}$ clusters to the central spectral region could not be excluded; fits for the 0.05 T spectra, but not the 8.0 T spectra, were improved by assuming that ~5% of the total Fe was in this form (with δ of 0.27 mm/s and ΔE_Q of 0.55 mm/s).

Respiring mitochondria exhibited a quadrupole doublet with δ of $\approx$0.83 mm/s and ΔE_Q of $\approx$2.4 mm/s, typical of HS Fe^{II} hemes (*36*). The dashed line above the spectrum of Figure 2A is a simulation of this species; its low-energy line is buried under the central doublet. The spectrum also contains a paramagnetic feature, best recognized after removing heme and central doublet contributions. The resulting absorption features (Figure 2B) at approximately 3.1 and −2.7 mm/s strongly suggest $S = {}^1/_2$ $[Fe_2S_2]^+$ clusters (due to the Rieske center in the bc_1 complex and the center in succinate dehydrogenase). Assuming the parameters of the Rieske protein (*37*) to simulate the contribution of a generic $S = {}^1/_2$ $[Fe_2S_2]^+$ cluster suggests that ~13% of the Fe in respiring mitochondria is present as such clusters. Analysis of Mössbauer and EPR spectra of another batch [R2 (Figure 4A and Figures S3 and S5 of the Supporting Information)] both yielded ~30 μM for

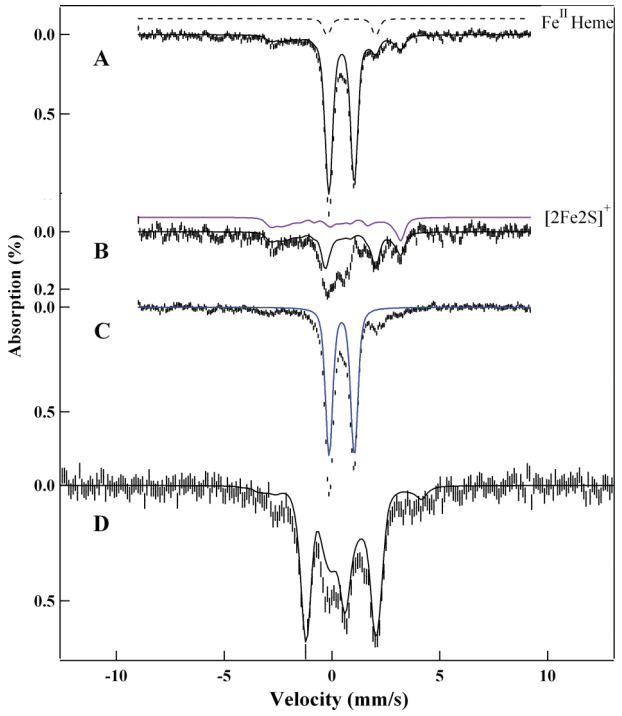

FIGURE 2: Mössbauer spectra of packed mitochondria (batch R1) isolated from respiring cells. (A) At ~5 K with a 0.05 T field applied parallel to the γ radiation. The black line is a simulation for the sum of the central doublet, HS Fe^{II} hemes (dashed), and $S = {}^1/_2$ $[Fe_2S_2]^+$ clusters. See Table 1 and the bar graph in Figure 7 for the percentages for all components. (B) Same as panel A after subtraction of the central doublet. The purple solid line is a simulation for $S = {}^1/_2$ $[Fe_2S_2]^+$ clusters, while the black solid line is a composite simulation including these species and HS Fe^{II} hemes. The absorption between 0 and 1 mm/s that is not covered by the black curve is unassigned. (C) Same as panel A but recorded at 100 K. The blue line outlines the contribution of the central doublet in the sample. (D) Same as panel A except at 4.2 K and with an 8.0 T parallel applied field. The black line is a simulation that includes the central doublet and contributions from $S = {}^1/_2$ $[Fe_2S_2]^+$ clusters.

this cluster type. At 100 K (Figure 2C), a portion of the magnetic pattern observed at ~5 K has collapsed, revealing that ≤2% of spectral intensity arises from NHHS Fe^{II} species ($\Delta E_Q \approx 3.0$ mm/s, and $\delta \approx 1.3$ mm/s). The black line on the 8.0 T data of Figure 2D simulates the central doublet and $S = {}^1/_2$ $[Fe_2S_2]^+$ clusters. After subtraction of the above-mentioned spectral features, some unresolved absorption remains at the center of the spectrum (Figure 2B) which could not be assigned unequivocally: a portion may be associated with Fe^{III} phosphate nanoparticles.

We previously reported that ~22% of the total Fe was present as non-heme Fe^{II} in respiring mitochondria grown on lactate (*1*). We now suspect that the majority of this was adventitious, as we no longer observe such features with this intensity in spectra of respiring mitochondria. Also, previously reported spectra (*1*) did not include a HS heme doublet, as we observe currently. In the initial stages of this project, samples were not isolated as rapidly as they are currently, and there may have been some heme and/or Fe−S cluster degradation that led to more intense non-heme HS Fe^{II} doublets.

Mitochondrial suspensions are turbid, leading to electronic absorption spectra with strong sloping baselines due to light scattering (Figure 3). Superimposed on this are Soret bands in the 400 nm region and α and β bands in the 500−620 nm region arising from both HS and LS Fe^{II} hemes (*35*). Spectra of respiring mitochondria were simulated (dashed lines in Figure 3A and

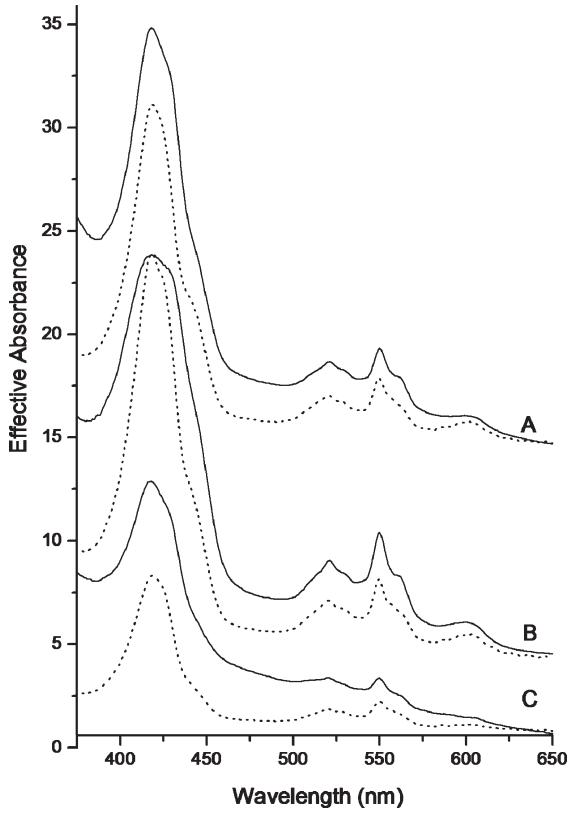

FIGURE 3: Electronic absorption spectra of mitochondrial suspensions: (A) respiring (R1), (B) respiro-fermenting (RF2), and (C) fermenting (F3). Effective absorbances of neat mitochondria normalized to a 10 mm path length cuvette are plotted. These values were obtained by multiplying raw absorbances by 2.0 (the dilution factor relative to packed mitochondria) and 5.0 (path length factor due to the use of a 2 mm path length cuvette) and by dividing by 0.82 (the packing factor). Dashed lines are composites from individual heme *a*-, *b*-, and *c*-containing proteins, using parameters listed in Table S1 of the Supporting Information (averages in Table 1).

Figure S4 of the Supporting Information) by adding spectra of individual heme *a*-, *b*-, and *c*-containing proteins (Figure S1 of the Supporting Information). Resulting concentrations (Table 1 and Table S2 of the Supporting Information) reveal the dominance of heme *c*, with hemes *b* and *a* present in roughly equal amounts. The HS fraction of these Fe^{II} hemes affords the heme Mössbauer doublet mentioned above, while the LS portion contributes to the central doublet.

EPR spectra of respiring mitochondria revealed additional details of the paramagnetic species observed by Mössbauer spectroscopy. The low-field region (Figure 4D) was dominated by $g \approx 6.0$ ($E/D = 0$) and $g = 6.4$ and 5.4 ($E/D \approx 0.021$) EPR signals; average spin concentrations are listed in Table 1. We assign these signals to the $\{a_3{:}Cu_b\}$ center of cytochrome *c* oxidase in which heme a_3 is Fe^{III} and Cu_b is Cu^I (*6*). The $g = 2$ region (Figure 4A) was dominated by signals with $g_{ave} = 1.95$ (2.03, 1.93, 1.91), $g_{ave} = 1.90$ (2.02, 1.90, 1.78), and $g_{ave} = 2.02$ (2.08, 1.99, 1.97) and a nearly isotropic signal with $g_{ave} = 2.01$ (perhaps combined with another signal at $g = 2.00$) (*1*). The dashed line in Figure 4A is the composite simulation. The $g_{ave} = 1.95$ and 1.90 signals have been assigned to the $[Fe_2S_2]^+$ clusters in succinate dehydrogenase (*38*) and the Rieske protein of cytochrome bc_1, respectively (*1*, *39*). The $g_{ave} = 2.01$ signal may originate from an $S = {}^1/_2$ $[Fe_3S_4]^+$ cluster, perhaps from the cluster in succinate dehydrogenase. The $g = 2.00$ signal probably arises from an organic-based radical. The $g_{ave} = 2.02$ feature may

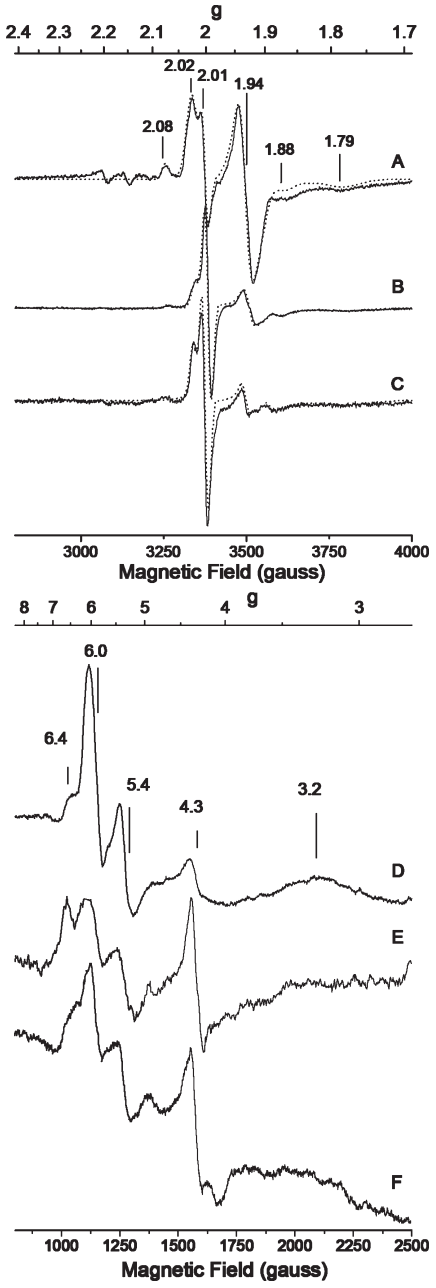

FIGURE 4: EPR spectra (10 K) of mitochondria from respiring (A, batch R2, decomposition in S5), respiro-fermenting (B, RF1), and fermenting (C, F11) cells. Spectra A and C were recorded at 0.05 mW, and spectrum B was recorded at 0.2 mW. Dashed lines are simulations, with batch-averaged parameters given in Table 1. Spectra D−F show the low-field regions of spectra A−C, respectively.

arise from ET flavoprotein-ubiquinone oxidoreductase (*40*). Minor resonances between $g = 2.2$ and $g = 2.1$ are often observed but remain unassigned. The bulk of the spin concentration in the $g = 2$ region belongs to $[Fe_2S_2]^+$ clusters that are most evident in Mössbauer spectra. The remainder belongs to minor species some of which may account for the unresolved background in the Mössbauer spectra. These results were generally similar to those reported for mitochondria isolated from yeast grown on glucose and lactate (*1*).

Respiro-Fermenting Mitochondria. Metal concentrations of mitochondria isolated from respiro-fermenting cells were similar to those of respiring mitochondria, except that the Mn concentration was 2-fold lower (Table 1). Mössbauer spectra (Figure 5) were also similar. Compared to respiring mitochondria,

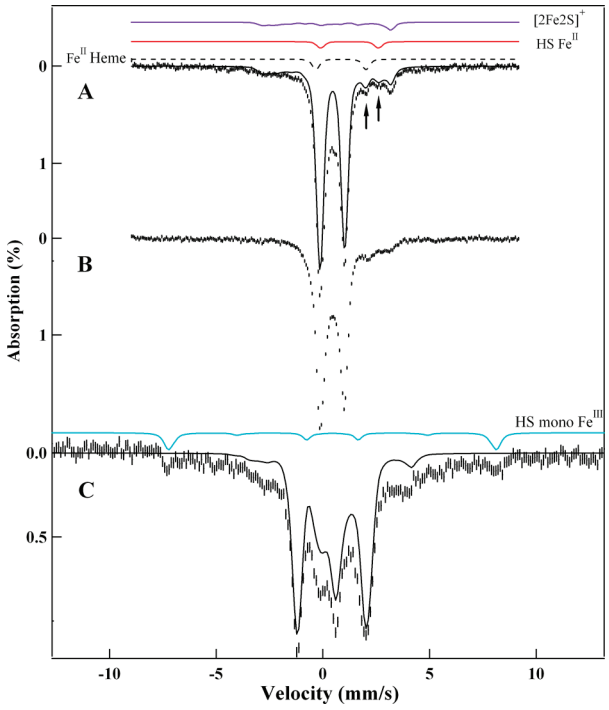

FIGURE 5: Mössbauer spectra of packed mitochondria (RF1) from respiro-fermenting cells. (A) Spectrum measured at ~5 K with a 0.05 T field applied parallel to the γ radiation. The black line is a simulation for the central doublet, HS Fe^{II} hemes, NHHS Fe^{II}, and $S = {}^1/_2$ $[Fe_2S_2]^+$ clusters. The lines above the spectrum are simulations for $S = {}^1/_2$ $[Fe_2S_2]^+$ (purple), non-heme HS Fe^{II} (red), and HS Fe^{II} heme (black dashed line). (B) Same as panel A but at 100 K. (C) Same as panel A but at 8.0 T and 4.2 K. The black line is a simulation for the central doublet and $S = {}^1/_2$ $[Fe_2S_2]^+$ clusters. The cyan line above is a simulation for HS mononuclear Fe^{III} species. See Table 1 for the concentrations of various species.

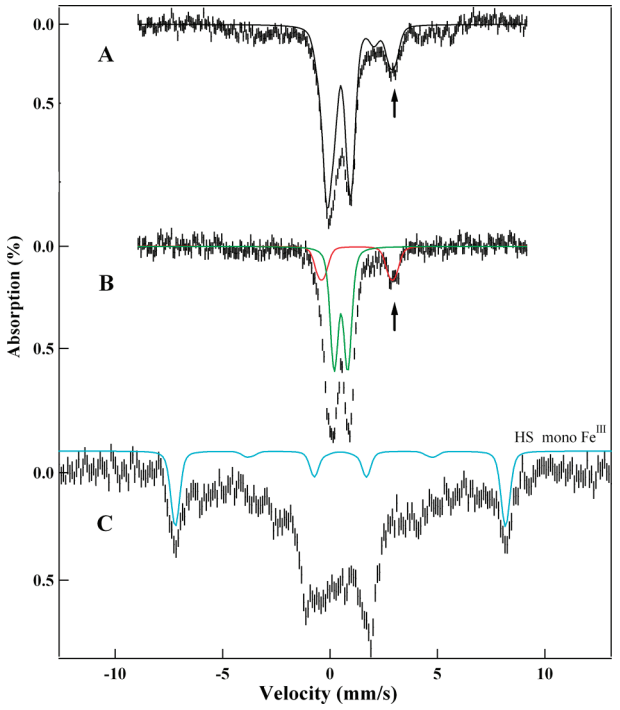

FIGURE 6: Mössbauer spectra of mitochondria (batch F9) from fermenting cells. (A) Spectrum measured at ~5 K with a 0.05 T field applied parallel to the γ radiation. The black line is a simulation for the sum of the central doublet, HS Fe^{II} hemes, NHHS Fe^{II} (high-energy line indicated by the arrow), and the Fe^{III} nanoparticles. (B) Same as panel A except at 100 K. The red line indicates HS Fe^{II}; the green line indicates the nanoparticle contribution (the doublet representing nanoparticles contains 20% of total Fe at ~5 K and 35% at 100 K; at 5 K the larger nanoparticles contribute a magnetically broadened spectrum). (C) Same as panel A except at 8.0 T and 4.2 K. The cyan line is a simulation for the HS Fe^{III}. See Table 1 for the concentrations of various species.

the proportion of Fe present as the central doublet, HS Fe^{II} hemes, and magnetic Fe in respiro-fermenting mitochondria declined slightly, while the percentages of NHHS Fe^{II} and the unassigned absorption in the center of the spectra increased slightly. A minor contribution of NHHS Fe^{II} (~2%) was assessed using the 100 K spectrum of Figure 5B. The presence of unassigned species is evident from the mismatch of the spectrum and simulation (Figure 5A) at ~0 mm/s. The 8.0 T spectrum reveals the presence of mononuclear HS Fe^{III} ions (Figure 5C, cyan line). The black line in Figure 5C is a simulation of the diamagnetic Fe associated with the central doublet at low field, together with a generic $S = {}^1/_2$ $[Fe_2S_2]^+$ cluster. EPR of a well-packed sample of the same batch yielded a spin concentration of 42 μM for the sum of the g_{ave} = 1.95 and 1.90 signals, suggesting that ~10% of the Fe belongs to $[Fe_2S_2]^+$ clusters. This value is similar to that suggested by the Mössbauer data. The electronic absorption spectrum of respiro-fermenting mitochondria (Figure 3B) revealed heme *a*, *b*, and *c* concentrations (Table 1) similar to those of respiring mitochondria.

Fermenting Mitochondria. Protein and Fe concentrations for fermenting mitochondria (Table 1) were again similar to those of respiring and respiro-fermenting mitochondria; the protein concentration might be reduced somewhat, but the variability was too high to establish this. The Mn concentration was similar to that in respiro-fermenting mitochondria and substantially lower than in respiring mitochondria. The Cu concentration was ~4-fold lower than those in respiring or respiro-fermenting mitochondria. Mössbauer spectra of fermenting mitochondria (Figure 6) are described in detail elsewhere (*29*); here we summarize that description. The spectra differed substantially from those of respiring or respiro-fermenting mitochondria in that there was a substantial decline in the fraction of Fe associated with the central doublet and an increase in the proportion of NHHS Fe^{II} and Fe^{III} nanoparticles (δ = 0.52 mm/s, and ΔE_Q = 0.63 mm/s). Electronic absorption spectra (Figure 3C and Figure S6 of the Supporting Information) exhibited lower concentrations of heme centers (Table 1 and Table S2 of the Supporting Information), consistent with the decline of the HS Fe^{II} heme doublet in Mössbauer spectra. EPR spectra of fermenting mitochondria (Figure 4C,F) were qualitatively similar to those of respiring and respiro-fermenting mitochondria, but with lower spin concentrations (Table 1). The g = 6 features, assigned to the partially oxidized a_3:Cu_b site of cytochrome *c* oxidase, declined as expected. Summing spin concentrations of the signals in the g = 2 region suggests that ≤3% of the Mössbauer spectral intensity should be associated with $S = {}^1/_2$ species, a fraction too small to be detected in the presence of increased amounts of NHHS Fe^{II} and ferric nanoparticles.

DISCUSSION

The main objective of this study was to characterize the distribution of the major Fe species in mitochondria isolated from respiring, respiro-fermenting, and fermenting yeast cells. In the following we integrate the results from the various techniques with the known composition of proteins in mitochondria, beginning with the respiring state. Our data allow an estimate of the

absolute concentration of cytochrome *c* oxidase in the organelle. As few other heme *a*-containing proteins are found in mitochondria, the heme *a* concentration essentially reflects twice the cytochrome *c* oxidase concentration. Mitochondrial heme monoxygenase may have substoichiometric amounts of heme *a* bound, but we will assume that this is insignificant. The total Fe^{II} heme *a* concentration in respiring mitochondria (Table 1, top part) suggests an average concentration of ~25 μM for cytochrome *c* oxidase with reduced heme *a* species (Table 1, bottom part). The absence of $g \sim 3$ EPR signals indicates the lack of LS Fe^{III} hemes in respiring mitochondria. Since cytochrome *c* oxidase contains 3 molar equiv of Cu, ~40% of the total Cu in respiring mitochondria should be in this enzyme. Most of the remainder might belong to a Cu^{I} pool (*31*). The percentage of mitochondrial Cu that we estimate for this pool (~60%) is smaller than the previous estimate (~90%). The absence of Cu^{II} EPR signals in our preparations is consistent with a Cu^{I} oxidation state for this pool.

The HS Fe^{II} heme quadrupole doublet of respiring mitochondria should include contributions from heme a_3- and HS heme *b*-containing proteins (we are unaware of any HS heme *c*-containing proteins). After subtraction of the heme a_3 contribution, the HS heme *b* species in respiring mitochondria (Table 1, bottom part) are likely to be found in cytochrome *c* peroxidase, catalase, and NO oxidoreductase, among others. Subtracting the HS heme *b* concentration from the total heme *b* concentration suggests that the concentration of LS heme *b* species in mitochondria is ~30 μM. These chromophores are found in succinate dehydrogenase (one heme *b*), cytochrome bc_1 (two heme *b* molecules), and others such as cytochrome b_2 and Cox15p. This can be described by the relationship

$$30\ \mu\text{M} = [\text{succinate dehydrogenase}] + 2[\text{cytochrome } bc_1] + \text{others}$$

As the spin concentrations for the $g_{ave} = 1.95$ and 1.90 EPR signals indicate the concentrations of succinate dehydrogenase (~5 μM) and cytochrome bc_1 (~10 μM), respectively, this relationship implies that most LS heme *b* centers in mitochondria reside in these two respiratory complexes.

The known heme *c*-containing proteins in mitochondria include cytochrome c_1 and two isoforms of cytochrome *c*. Removing the cytochrome bc_1 concentration suggests that the collective concentration of the isoforms is ~110 μM. This indicates that the heme *a* and *c* contents of respiring mitochondria are dominated by cytochrome *c* oxidase and cytochrome *c*, respectively. The heme *b* content is more evenly distributed between HS and LS, with LS forms dominated by succinate dehydrogenase and cytochrome bc_1. Concentrations in Table 1 (bottom part) were calculated with respect to the entire mitochondrial volume. Since species are located in particular regions of the mitochondria, their regional concentrations will be higher.

Succinate dehydrogenase contains 10 molar equiv of Fe (one LS heme *b*, one Fe_2S_2 cluster, one Fe_3S_4 cluster, and one Fe_4S_4 cluster), so a concentration of ~5 μM for this respiratory complex implies an ~50 μM Fe contribution overall. Similarly, cytochrome bc_1 contains 5 molar equiv of Fe (one heme c_1, two heme *b* molecules, and one Fe_2S_2 cluster), also implying an ~50 μM overall Fe contribution. Including a 60 μM Fe contribution for cytochrome *c* oxidase and 110 μM for cytochrome *c* reveals that respiration-related complexes constitute ~40% of the iron in respiring yeast mitochondria.

The central doublet of the Mössbauer spectra of respiring mitochondria includes contributions from $[Fe_4S_4]^{2+}$ clusters and

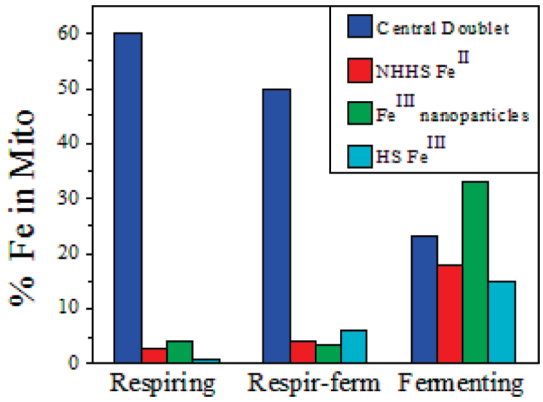

FIGURE 7: Bar graph showing the major forms of Fe present in respiring, respiro-fermenting, and fermenting mitochondria. Color-coding is matched to simulated features in previous Mössbauer figures.

LS Fe^{II} hemes. Table 1 and the relationships mentioned above suggest ~30 μM (LS heme *a*) + ~30 μM (LS heme *b*) + ~120 μM (LS heme *c*) = ~180 μM LS Fe^{II} hemes. Subtracting this from the central doublet leaves ~35% of the mitochondrial Fe in the form of $S = 0$ $[Fe_4S_4]^{2+}$ clusters. This corresponds to ~250 μM Fe or to ~60 μM of such clusters. Subtracting an additional 5 μM contribution due to the succinate dehydrogenase $[Fe_4S_4]^{2+}$ cluster leaves ~55 μM for Fe_4S_4 clusters in other mitochondrial proteins.

Some mitochondrial proteins contain only Fe_4S_4 clusters; some contain only Fe_2S_2 clusters, and some contain both cluster types. We have attempted to fit simulations of oxidized $[Fe_2S_2]^{2+}$ clusters into the Mössbauer spectra of respiring mitochondria, but we have no clear evidence of their presence. This suggests for respiring mitochondria that the majority of $[Fe_4S_4]^{2+}$ clusters that are not contained in succinate dehydrogenase reside in proteins that contain only $[Fe_4S_4]^{2+}$ clusters.

Respiro-fermenting and fermenting mitochondria were analyzed similarly (Table 1, bottom part); results are summarized by the bar chart in Figure 7. In general, the total Fe concentration was similar regardless of metabolic mode. Also, the overall distribution of Fe in respiro-fermenting mitochondria was similar to that in respiring mitochondria. In contrast, the Fe distribution in fermenting mitochondria was dramatically different. This suggests that the repression of respiration by glucose, rather than the occurrence of fermentation per se, is responsible for the major shifts observed in Fe distribution. Thus, we will simplify our further analysis by averaging the Fe distributions observed for respiring and respiro-fermenting mitochondria and then compare this to the distribution obtained under fermentation.

Viewed in the respiration → fermentation direction, cytochrome *c* oxidase ↓ (declined) 4-fold, succinate dehydrogenase ↓ 3.8-fold, cytochrome bc_1 ↓ 2.5-fold, cytochrome *c* ↓ 2-fold, LS hemes generally ↓ 2-fold, and $[Fe_4S_4]^{2+}$ cluster-containing proteins ↓ 3.5-fold. The Cu^{I} pool decreased 3-fold. The decline in the size of the Cu^{I} pool upon shifting from respiration to fermentation contrasts with a previous report (*31*) that the concentration of this pool is independent of metabolic growth mode. In terms of Fe pools, the NHHS Fe^{II} pool, the mononuclear HS Fe^{III} pool, and the Fe^{III} nanoparticles went from nearly undetectable in respiring mitochondria to representing ~75% of the Fe in the fermenting organelle. These dramatic changes reflect major differences in the way that Fe is handled by the cell, depending on metabolic mode.

We do not know the location of these pools within mitochondria but suspect that they are located in the matrix. Nor are the ligands coordinating the Fe in these pools known. The ferric ions in the Fe^{III} nanoparticles found in Atm1-depleted mitochondria appear to be coordinated by ligands with oxygen donors but essentially lacking in N, S, or C atoms (*41*). Phosphate, water, and hydroxide ligands were suggested as likely ligands in these nanoparticles, and similar ligands might be associated with the nanoparticles observed in mitochondria from wild-type fermenting cells. The non-heme high-spin Fe^{II} pool may consist of multiple species. Some mitochondrial proteins (e.g., frataxin, ferrochelatase, Fe−S cluster scaffold proteins, and CoQ7) may coordinate HS Fe^{II} ions, but the collective concentration of these proteins may be insufficient to account for the overall concentration of the NHHS Fe^{II} pool (~150 μM in fermenting mitochondria). Seguin et al. (*42*) determined that yeast cells grown under similar conditions contained ~1300 copies of Yfh1p. If we assume 60×10^{-15} L for the volume of a yeast cell (*43*−*46*), that 3% of that volume was due to mitochondria (*47*, *48*), and that each Yfh1p bound two Fe^{II} ions (*49*), this would correspond to a concentration of ~70 nM. Even if there were a dozen such proteins in mitochondria, their collective concentration would be 2 orders of magnitude lower than that present in the NHHS Fe^{II} pool of fermenting mitochondria. These considerations strongly suggest that the nonheme HS Fe^{II} pool is dominated by nonproteinaceous low-molecular weight complexes.

The results of this study can be compared to those of proteomic studies that also indicate substantial changes in the yeast mitochondria proteome due to the diauxic shift (*23*). The concentrations of 17 proteins are significantly lower in fermenting versus respiring cells, including cytochrome *c* oxidase, cytochrome bc_1, and succinate dehydrogenase (*50*). The mitochondrial transcriptome changes more dramatically, with levels of transcripts of cytochrome *c* isoform 1 and Mn-superoxide dismutase (MnSod2) declining under fermentation (*51*, *52*). Other groups have also reported lower SOD2 protein and transcript levels under fermentation (*53*, *54*). Our results are consistent, including the 3-fold increase in the Mn concentration of respiring mitochondria relative to respiro-fermenting and fermenting conditions which might reflect changes in the levels of MnSod2 or associated Mn species.

The observed changes in the distribution of Fe in mitochondria isolated from cells grown under different metabolic modes can be interpreted given the known roles of mitochondria in respiring versus fermenting cells. In respiring cells, these organelles are critical for energy production, which requires the biosynthesis of Fe−S clusters and heme centers, as well as their installation into apo-respiratory complexes. Under fermentation conditions, energy production is associated with glycolysis, where no such centers are involved. Thus, the level of production of Fe−S clusters and heme centers is probably reduced in fermenting mitochondria because the metabolic need for these centers is reduced. Our results suggest a 3-fold reduction in these centers. Residual amounts of such centers might allow fermenting cells to convert rapidly into respiration mode as environmental conditions change.

The Fe used to synthesize mitochondrial Fe−S clusters and hemes is imported into the organelle as Fe^{II} (*55*). Neither the structure nor the composition of the imported complex(es) is(are) known, but each is probably of low molecular weight as each must pass through transporters in the IM (*3*). We propose that

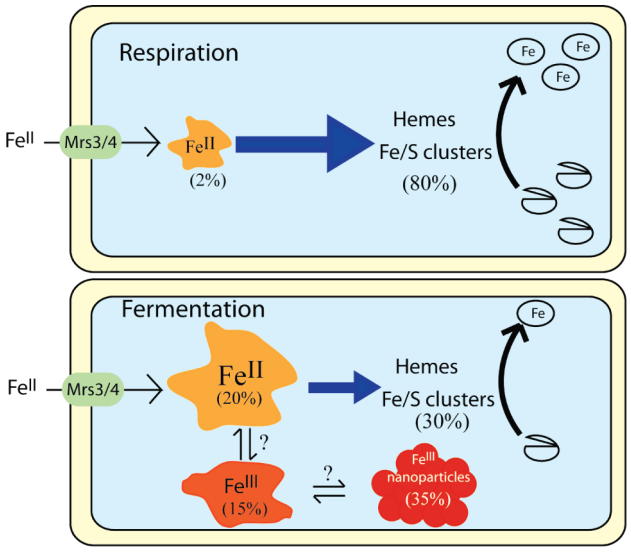

FIGURE 8: Model describing the shift in the iron content of mitochondria with metabolic growth mode. The size of the NHHS Fe^{II} pool is dictated by the balance of input and output fluxes. During respiration, the pool is small (~15 μM). When cells ferment, the rate of Fe−S cluster and heme biosynthesis declines, causing the pool to enlarge (~150 μM). The rate of import of Fe^{II} from the cytosol is not significantly affected by the change in metabolism. Under fermenting conditions, a portion of the NHHS Fe^{II} pool may become oxidized to mononuclear non-heme HS Fe^{III}, a subset of which may precipitate as Fe^{III} nanoparticles.

the non-heme HS Fe^{II} ions present in fermenting mitochondria are these imported ions and that they serve in this capacity. The simple model of Figure 8 assumes this role and can rationalize the observed changes in the level of this pool. During respiration, the size of the Fe^{II} pool is small since the biosynthesis rates of Fe−S clusters and hemes are elevated. During fermentation, the pool increases because the rate of Fe−S cluster and heme biosynthesis is diminished. Consistent with the nearly invariant Fe concentrations in respiring and fermenting mitochondria, the overall rate of Fe^{II} import appears to be unaffected by changes in metabolic growth mode; i.e., the cell does not seem to regulate the rate of import of Fe^{II} into mitochondria according to metabolic growth mode. Understanding Fe fluxes at the cellular level will require that the different percentage volumes occupied by mitochondria in fermenting versus respiring cells be taken into account. Another uncertainty, at the mitochondrial level, is the relationship between the NHHS Fe^{II} pool and the other pools of Fe in fermenting mitochondria, including Fe^{III} nanoparticles, mononuclear HS Fe^{III} ions, and the central unresolved material. The three pools may exist in a dynamic equilibrium with each other, or they might be independent (e.g., imported by different IM transporters). Also uncertain is the cellular function of these other pools. They certainly store Fe in fermenting mitochondria, and the absence of these pools during respiration suggests either that these pools can be utilized under respiratory growth conditions or that they never form under these conditions. However, whether this is a cellular *strategy* for storing Fe, analogous to mitoferrin in human mitochondria (*56*), is uncertain. These pools may possibly result from an insufficient concentration of a coordinating ligand or a shift of either pH or oxidation status in fermenting mitochondria. We favor this latter characterization especially for the Fe^{III} nanoparticle pool, in that the ligands coordinating these ions are probably not protein-bound and thus would not be under the direct genetic

control of the cell. Nevertheless, this pool may indirectly impact cellular function, e.g., by generating reactive oxygen species during its formation, and it may be bioavailable under particular metabolic conditions.

ACKNOWLEDGMENT

We thank Dr. Graham Palmer (Rice University) for generously providing a digital spectrum of cytochrome *c* oxidase and Dr. Carla Koehler (University of California, Los Angeles, CA) for kindly providing the cytochrome *c* antibody.

SUPPORTING INFORMATION AVAILABLE

Protein and metal concentrations in isolated mitochondria (Table S1), electronic absorption spectra of heme-containing proteins (Figure S1), protection of cytochrome *c* from protease degradation in isolated mitochondria (Figure S2), Mössbauer spectra of a respiring mitochondrial batch not shown in Figure 2 but used in constructing Table 1 (Figure S3), electronic absorption spectra of respiring mitochondrial suspensions (Figure S4), concentrations of each heme component determined for individual mitochondrial samples (Table S2), 10 K EPR spectra of mitochondria batches not shown in Figure 4 but used in the construction of Table 1 (Figure S5), and electronic absorption spectra of different batches of fermenting mitochondria (Figure S6). This material is available free of charge via the Internet at http://pubs.acs.org.

REFERENCES

1. Hudder, B. N., Morales, J. G., Stubna, A., Münck, E., Hendrich, M. P., and Lindahl, P. A. (2007) Electron paramagnetic resonance and Mössbauer spectroscopy of intact mitochondria from respiring *Saccharomyces cerevisiae*. *J. Biol. Inorg. Chem. 12*, 1029–1053.
2. Lindahl, P. A., Morales, J. G., Miao, R., and Holmes-Hampton, G. (2009) Isolation of *Saccharomyces cerevisiae* mitochondria for Mössbauer, EPR, and electronic absorption spectroscopic analyses. *Methods Enzymol. 456*, 267–285.
3. Lill, R., and Mühlenhoff, U. (2008) Maturation of iron-sulfur proteins in eukaryotes: Mechanisms, connected processes, and diseases. *Annu. Rev. Biochem. 77*, 669–700.
4. Beinert, H. (2002) Spectroscopy of succinate dehydrogenases, a historical perspective. *Biochim. Biophys. Acta 1553*, 7–22.
5. Hunte, C., Koepke, J., Lange, C., Rossmanith, T., and Michel, H. (2000) Structure at 2.3 angstrom resolution of the cytochrome bc_1 complex from the yeast *Saccharomyces cerevisiae* co-crystallized with an antibody Fv fragment. *Structure 8*, 669–684.
6. Beinert, H., and Shaw, R. W. (1977) On Identitiy of High-Spin Heme Components of Cytochrome-C Oxidase. *Biochim. Biophys. Acta 462*, 121–130.
7. Barrientos, A. (2003) Yeast Models of Human Mitochondrial Diseases. *IUBMB Life 55*, 85–95.
8. Irazusta, V., Moreno-Cermeño, A., Cabiscol, E., Ros, J., and Tamarit, J. (2008) Major targets of iron-induced protein oxidative damage in frataxin-deficient yeasts are magnesium-binding proteins. *Free Radical Biol. Med. 44*, 1712–1723.
9. Rouault, T. A., and Tong, W.-H. (2008) Iron−sulfur cluster biogenesis and human disease. *Trends Genet. 24*, 398–407.
10. Veatch, J. R., McMurray, M. A., Nelson, Z. W., and Gottschling, D. E. (2009) Mitochondrial Dysfunction Leads to Nuclear Genome Instability via an Iron-Sulfur Cluster Defect. *Cell 137*, 1247–1258.
11. Huang, M. E., and Kolodner, R. D. (2005) A biological network in *Saccharomyces cerevisiae* prevents the deleterious effects of endogenous oxidative DNA damage. *Mol. Cell 17*, 709–720.
12. Barja, G. (1998) Mitochondrial free radical production and aging in mammals and birds (Harman, D., Holliday, R., and Meydani, M., Eds.) pp 224−238, New York Academy of Sciences, New York.
13. Raha, S., McEachern, G. E., Myint, A. T., and Robinson, B. H. (2000) Superoxides from mitochondrial complex III: The role of manganese superoxide dismutase. *Free Radical Biol. Med. 29*, 170–180.
14. Turrens, J. F. (1997) Superoxide production by the mitochondrial respiratory chain. *Biosci. Rep. 17*, 3–8.
15. Scheffler, I. E. (1999) Mitochondria, Wiley-Liss, New York.
16. Babcock, M., deSilva, D., Oaks, R., DavisKaplan, S., Jiralerspong, S., Montermini, L., Pandolfo, M., and Kaplan, J. (1997) Regulation of mitochondrial iron accumulation by Yfh1p, a putative homolog of frataxin. *Science 276*, 1709–1712.
17. Carraway, M. S., Suliman, H. B., Madden, M. C., Piantadosi, C. A., and Ghio, A. J. (2006) Metabolic capacity regulates iron homeostasis in endothelial cells. *Free Radical Biol. Med. 41*, 1662–1669.
18. Lesuisse, E., Santos, R., Matzanke, B. F., Knight, S. A. B., Camadro, J. M., and Dancis, A. (2003) Iron use for haeme synthesis is under control of the yeast frataxin homologue (Yfh1). *Hum. Mol. Genet. 12*, 879–889.
19. Napoli, E., Taroni, F., and Coropassi, G. A. (2006) Frataxin, Iron−Sulfur Clusters, Heme, ROS, and Aging. *Antioxid. Redox Signaling 8*, 506–516.
20. Hare, D., Reedy, B., Grimm, R., Wilkins, S., Volitakis, I., George, J. L., Cherny, R. A., Bush, A. I., Finkelstein, D. I., and Doble, P. (2009) Quantitative elemental bio-imaging of Mn, Fe, Cu and Zn in 6-hydroxydopamine induced Parkinsonism mouse models. *Metallomics 1*, 53–58.
21. Lee, D. W., Kaur, D., Chinta, S. J., Rajagopalan, S., and Andersen, J. K. (2009) A Disruption in Iron-Sulfur Center Biogenesis via Inhibition of Mitochondrial Dithiol Glutaredoxin 2 May Contribute to Mitochondrial and Cellular Iron Dysregulation in Mammalian Glutathione-Depleted Dopaminergic Cells: Implications for Parkinson's Disease. *Antioxid. Redox Signaling 11*, 2083–2094.
22. Camaschella, C., Campanella, A., De Falco, L., Boschetto, L., Merlini, R., Silvestri, L., Levi, S., and Iolascon, A. (2007) The human counterpart of zebrafish shiraz shows sideroblastic-like microcytic anemia and iron overload. *Blood 110*, 1353–1358.
23. Schonauer, M. S., and Dieckmann, C. L. (2004) Mitochondrial genomics and proteomics. *Curr. Genomics 5*, 575–588.
24. Münck, E., Sidney, F., and Lester, P. (1978) Mössbauer spectroscopy of proteins: Electron carriers. *Methods Enzymol. 54*, 346–379.
25. Stevens, B. J. (1977) Variation in Number and Volume of Mitochondria in Yeast According to Growth-Conditions: Study Based on Serial Sectioning and Computer Graphics Reconstitution. *Biol. Cell. 28*, 37–56.
26. Egner, A., Jakobs, S., and Hell, S. W. (2002) Fast 100-nm resolution three-dimensional microscope reveals structural plasticity of mitochondria in live yeast. *Proc. Natl. Acad. Sci. U.S.A. 99*, 3370–3375.
27. Miao, R., Martinho, M., Morales, J. G., Kim, H., Ellis, E. A., Lill, R., Hendrich, M. P., Münck, E., and Lindahl, P. A. (2008) EPR and Mössbauer spectroscopy of intact mitochondria isolated from Yah1p-depleted *Saccharomyces cerevisiae*. *Biochemistry 47*, 9888–9899.
28. Sherman, F. (1991) Getting Started with Yeast. *Methods Enzymol. 194*, 3–21.
29. Holmes-Hampton, G. P., Miao, R., Garber-Morales, J., Guo, Y., Münck, E., and Lindahl, P. A. (2010) A nonheme high-spin ferrous pool in mitochondria from fermenting *Saccharomyces cerevisiae*. *Biochemistry 49*, 4227–4234.
30. Dabir, D. V., Leverich, E. P., Kim, S. K., Tsai, F. D., Hirasawa, M., Knaff, D. B., and Koehler, C. M. (2007) A role for cytochrome c and cytochrome c peroxidase in electron shuttling from Erv1. *EMBO J. 26*, 4801–4811.
31. Cobine, P. A., Ojeda, L. D., Rigby, K. M., and Winge, D. R. (2004) Yeast contain a non-proteinaceous pool of copper in the mitochondrial matrix. *J. Biol. Chem. 279*, 14447–14455.
32. Foury, F., and Cazzalini, O. (1997) Deletion of the yeast homologue of the human gene associated with Friedreich's Ataxia elicits iron accumulation in mitochondria. *FEBS Lett. 411*, 373–377.
33. Kispal, G., Csere, P., Prohl, C., and Lill, R. (1999) The mitochondrial proteins Atm1p and Nfs1p are essential for biogenesis of cytosolic FeS proteins. *EMBO J. 18*, 3981–3989.
34. Tangeras, A., Flatmark, T., Backstrom, D., and Ehrenberg, A. (1980) Mitochondrial Iron Not Bound in Heme and Iron-Sulfur Centers: Estimation, Compartmentation and Redox State. *Biochim. Biophys. Acta 589*, 162–175.
35. Liao, G. L., and Palmer, G. (1996) The reduced minus oxidized difference spectra of cytochromes a and a_3. *Biochim. Biophys. Acta 1274*, 109–111.
36. Wang, H., Sauke, T., Debrunner, P. G., and Chan, S. I. (1988) The CO Adduct of Yeast Cytochrome-C Oxidase: Mössbauer and Photolysis Studies. *J. Biol. Chem. 263*, 15260–15263.
37. Pikus, J. D., Studts, J. M., Achim, C., Kauffmann, K. E., Münck, E., Steffan, R. J., McClay, K., and Fox, B. G. (1996) Recombinant toluene-4-monooxygenase: Catalytic and Mössbauer studies of the

purified diiron and Rieske components of a four-protein complex. *Biochemistry 35*, 9106–9119.
38. Maguire, J. J., Johnson, M. K., Morningstar, J. E., Ackrell, B. A. C., and Kearney, E. B. (1985) Electron-Paramagnetic Rresonance Studies of Mammalian Succinate-Dehyrogenase Detection of the Tetranuclear Cluster S2. *J. Biol. Chem. 260*, 909–912.
39. Fee, J. A., Findling, K. L., Yoshida, T., Hille, R., Tarr, G. E., Hearshen, D. O., Dunham, W. R., Day, E. P., Kent, T. A., and Münck, E. (1984) Purification and Characterization of the Rieske Iron-Sulfur Protein from *Thermus thermophilus*: Evidence for a [2Fe-2S] Cluster Having Non-Cysteine Ligands. *J. Biol. Chem. 259*, 124–133.
40. Swanson, M. A., Usselman, R. J., Frerman, F. E., Eaton, G. R., and Eaton, S. S. (2008) The iron-sulfur cluster of electron transfer flavoprotein-ubiquinone oxidoreductase is the electron acceptor for electron transfer flavoprotein. *Biochemistry 47*, 8894–8901.
41. Miao, R., Kim, H., Koppolu, U. M. K., Ellis, E. A., Scott, R. A., and Lindahl, P. A. (2009) Biophysical Characterization of the Iron in Mitochondria from Atm1p-Depleted *Saccharomyces cerevisiae*. *Biochemistry 48*, 9556–9568.
42. Seguin, A., Bayot, A., Dancis, A., Rogowska-Wrzesinska, A., Auchere, F., Camadro, J. M., Bulteau, A. L., and Lesuisse, E. (2009) Overexpression of the yeast frataxin homolog (Yfh1): Contrasting effects on iron-sulfur cluster assembly, heme synthesis and resistance to oxidative stress. *Mitochondrion 9*, 130–138.
43. Jorgensen, P., Nishikawa, J. L., Breitkreutz, B. J., and Tyers, M. (2002) Systematic identification of pathways that couple cell growth and division in yeast. *Science 297*, 395–400.
44. Sherman, F. (2002) Getting started with yeast. *Methods Enzymol. 350*, 3–41.
45. Tamaki, H., Yun, C. W., Mizutani, T., Tsuzuki, T., Takagi, Y., Shinozaki, M., Kodama, Y., Shirahige, K., and Kumagai, H. (2005) Glucose-dependent cell size is regulated by a G protein-coupled receptor system in yeast *Saccharomyces cerevisiae*. *Genes Cells 10*, 193–206.
46. Tyson, C. B., Lord, P. G., and Wheals, A. E. (1979) Dependency of Size of *Saccharomyces cerevisiae* Cells on Growth Rate. *J. Bacteriol. 138*, 92–98.
47. Polakis, E. S., Bartley, W., and Meek, G. A. (1964) Changes in Structure + Enzyme Activity of *Saccharomyces cerevisiae* in Response to Changes in Environment. *Biochem. J. 90*, 369.
48. Polakis, E. S., Bartley, W., and Meek, G. A. (1965) Changes in Activities of Respiratory Enzymes during Aerobic Growth of Yeast on Different Carbon Sources. *Biochem. J. 97*, 298.
49. Cook, J. D., Bencze, K. Z., Jankovic, A. D., Crater, A. K., Busch, C. N., Bradley, P. B., Stemmler, A. J., Spaller, M. R., and Stemmler, T. L. (2006) Monomeric yeast frataxin is an iron-binding protein. *Biochemistry 45*, 7767–7777.
50. Ohlmeier, S., Kastaniotis, A. J., Hiltunen, J. K., and Bergmann, U. (2004) The Yeast Mitochondrial Proteome, a Study of Fermentative and Respiratory Growth. *J. Biol. Chem. 279*, 3956–3979.
51. Costa, V., Amorim, M. A., Reis, E., Quintaniha, A., and Moradas-Ferreira, P. (1979) Mitochondrial superoxide dismutase is essential for ethanol tolerance of *Saccharomyces cerevisiae* in the post-diauxic phase. *Microbiology 143*, 1649–1656.
52. Zitomer, R. S., Montgomery, D. L., Nichols, D. L., and Halo, B. D. (1979) Transcriptional regulation of the yeast cytochrome c gene. *Proc. Natl. Acad. Sci. U.S.A. 76*, 3627–3631.
53. Macierzynska, E., Grzelak, A., and Bartosz, G. (2007) The effect of growth medium on the antioxidant defense of *Saccharomyces cerevisiae*. *Cell. Mol. Biol. Lett. 12*, 448–456.
54. Maris, A. F., Assumpcao, A. L. K., Bonatto, D., Brendel, M., and Henriques, J. A. P. (2001) Diauxic shift-induced stress resistance against hydroperoxides in *Saccharomyces cerevisiae* is not an adaptive stress response and does not depend on functional mitochondria. *Curr. Genet. 39*, 137–149.
55. Lange, H., Kispal, G., and Lill, R. (1999) Mechanism of iron transport to the site of heme synthesis inside yeast mitochondria. *J. Biol. Chem. 274*, 18989–18996.
56. Paradkar, P. N., Zumbrennen, K. B., Paw, B. H., Ward, D. M., and Kaplan, J. (2009) Regulation of Mitochondrial Iron Import through Differential Turnover of Mitoferrin 1 and Mitoferrin 2. *Mol. Cell. Biol. 29*, 1007–1016.